Localized fluoride diffusion and defect equilibrium in CaF_2:Eu^{3+} using site-selective spectroscopy and high-pressure techniques

Lawrence R. Olsen,* Andrew O. Wright,† and John C. Wright‡
Department of Chemistry, University of Wisconsin at Madison, Madison, Wisconsin 53706
(Received 3 November 1995)

Crystals of CaF_2:Eu^{3+} were treated at high pressure and temperature in a diamond-anvil cell to produce a nonequilibrium distribution of the charge-compensating interstitial fluorides. The reequilibration dynamics were then studied by annealing the treated sample at normal pressure. The reequilibration of the fluorides spanned an 80° temperature range, which corresponds to a 0.34-eV range of diffusional activation energies based on a kinetic simulation of the experiment. Spectroscopic techniques were used to measure the major sites and several previously unreported minor defect clusters. The changes in the main sites correlate with changes in the minor clusters. A model for the distribution and properties of defects in CaF_2:Eu is proposed, and the implications of the model are discussed. [S0163-1829(96)05822-5]

Compounds with fluorite crystal structure have been the subject of extensive study. There are several reasons for the interest in these solids. The fluorite structure contains large interstitial sites, which facilitate the formation of anion Frenkel defects. Because of the low enthalpy for defect formation, many of the compounds can be used as ion conductors at moderate temperatures.

CaF_2 doped with trivalent rare earths is often used as a model system for the fluorites. The rare-earth atoms substitute for calcium, and must be charge compensated by an additional fluoride interstitial. Defect structures formed by rare-earth dopants and fluoride interstitials have been studied, as well as the anion kinetics in both doped and undoped samples.[1–4] Despite the work which has been done, there are still discrepancies in experimental results and the interpretation of them.

The analysis of many experiments has been based on the simple dissociation of rare-earth–fluoride pairs to form an isolated cubic rare-earth site and a free interstitial fluoride. Experiments, however, have shown that there is an anomalous relationship between dopant concentration and the ratio of paired to cubic sites for concentrations above 0.1 mole %.[5,6] The primary reason for the anomaly is the trapping of free interstitial fluorides by other defect sites. Energy calculations indicate that the cation dimer should strongly bond to a third interstitial fluoride, and kinetic studies confirm that both the dimer and trimer clusters have extra fluoride ions.[7,8] Many experiments measuring anion kinetics have used doped crystals containing a variety of cluster sites, but the data interpretation has neglected the presence of the clusters.[3,4] A better understanding of how these competing equilibria affect the distribution and the mobilities of the anions is needed for interpreting experimental results.

In the first part of this experiment, site-selective spectroscopy is used to identify and characterize the defects present in samples of CaF_2 doped with between 0.1 and 1.0-mole % europium. Several additional defects sites are identified.

In the second part, high pressure from a diamond-anvil cell produces a nonequilibrium distribution of the interstitial fluorides in the lattice. Concentration changes in the single pair and dissociated cubic sites are correlated with changes in several of the minor cluster sites.

In the final part of the experiment, the reequilibration kinetics are studied by annealing the crystal at normal pressure and increasing temperatures. A computer simulation is used to match defect and diffusional parameters to the annealing data. A model for defect interactions in the crystal is proposed which reproduces the behavior of the major and minor sites, and explains the extended temperature range of the reequilibration process.

BACKGROUND

Rare-earth ions readily substitute into CaF_2 and related compounds without altering the overall cubic symmetry of the lattice. When oxygen is excluded, the excess charge of the trivalent rare-earth ion is compensated for by an interstitial fluoride, which can be either bound to the defect or located distantly. For europium, the main sites seen spectroscopically are the single europium features A, O, and P, and the cluster sites labeled R and Q.[9] The A site has tetragonal symmetry, and has been identified as having a fluoride in the nearest-neighbor interstitial position.[10] This site can be represented as $(Eu\cdot F)^x$, where the use of the superscripts $\cdot$, $'$, and x are used to indicate a net positive, negative, or neutral charge with respect to the lattice. The O site has cubic symmetry and must be charge compensated by an excess fluoride at a distant location. The P-site intensity is generally small, and it may be related to impurities in the samples. A trigonal $(Eu\cdot F)^x$ site with a fluoride in the next-nearest-neighbor position is seen in fluorites doped with smaller rare-earth ions, but it is usually not observed in CaF_2:Eu. The R and the Q centers are the $(2Eu\cdot 3F)'$ dimer and the $(3Eu\cdot 4F)'$ trimer, respectively.[8] For smaller rare-earth ions, there is evidence of larger clusters.[11]

Site-selective spectroscopy is a versatile tool for studying these rare-earth defects. The f-f orbital transitions are well shielded from the lattice, giving long fluorescent lifetimes and sharp atomiclike spectral lines at low temperatures. The crystal-field splitting gives information about the symmetry

of a site, and the relaxation rates give information about clustering. By using a monochromator to monitor specific fluorescent features while simultaneously scanning a tunable laser over absorption features, it is possible to correlate the fluorescence and absorption lines belonging to a rare-earth site.

The cation dopants are able to diffuse at temperatures above 530 °C in CaF_2.[6] At annealing temperatures below 600 °C the distribution of defects is controlled by the enthalpy term in the free energy, and the final equilibrium distribution is largely dominated by clusters. In samples quenched from above 800 °C the distribution is dominated by single-ion sites. The crystals used in this experiment were quenched from high temperatures to reduce the clustering and simplify the defect distribution. Our primary concerns were with the distribution and kinetics of the interstitial fluoride ions, and how these correlated with the concentration anomaly for the *A* and *O* sites.

Fluorides ions are mobile near room temperature, which limits the extent to which a nonequilibrium distribution of the fluorides can be obtained by thermal quenching. To avoid this limitation, samples were placed under high hydrostatic pressure in a diamond-anvil cell. In the compressed lattice the interstitial fluorides move to sites that minimize strain energies. The pressure also reduces the mobility of the fluorides, so the cell was heated to enable the formation of this altered equilibrium. The fluoride distribution was frozen in by cooling the cell below room temperature. The pressure was then released, the reequilibration was studied under standard conditions.

EXPERIMENT

The crystals used in this study were obtained commercially from Optovac, Inc. Two of the crystals were from a previous study, where the Eu^{3+} concentrations were determined to be 0.09 and 0.19 mole %.[8] The third crystal has a nominal europium concentration of 1.0%. To minimize the concentration of defect clusters, the samples were heated in evacuated Vycor tubes at high temperature (804 °C for the 0.09% sample, 890 °C for the others) for 12 h, quenched, and checked for oxygen contamination.[12]

For the first part of the experiment, the sample crystals were mounted using copper-impregnated grease on a copper holder, and placed on the cold finger of a closed cycle helium refrigerator which can regulate temperature between 12 and 350 K. For the annealing portion of the experiment the small crystal chips could either be transferred to cavities in a special holder, or left in the diamond-anvil cell (DAC), which attached to the refrigerator.

The diamond-anvil cell was a clamped piston-cylinder design made from inconel by Diacell Products.[13] The diamonds were originally mounted using a ceramic cement, but the cement lost adhesion after temperature cycling and was replacing with fitted retainers.

The diamond culets had octagonal 700-μm faces. A rhenium-molybdenum alloy was used for the gaskets to maintain containment strength at high temperatures, and also to prevent welding of the metal to the diamonds.[14] The gasket material was a 250-μm sheet which was preindented and then drilled with a 250-μm carbide bit. After pressure application the gasket cavity was typically 150×90 μm^2 deep. This cell design should allow us to reach pressures of 150 kbar, but we found that clamping at high temperature gave more modest final pressures of around 40 kbar.

70-μm sample chips taken from the reference crystal were used in the experiment. A ruby chip was also loaded into the cell for pressure determination, and a pentane-isopentante mix was used for the pressure medium. This mix is hydrostatic at these pressures,[15] and should not risk introducing oxygen into the CaF_2 lattice when used at high temperatures. For the high-temperature-pressurized treatments, the DAC was mounted inside a vacuum oven. The oven is a simplified version of the Shifferel design,[14] and includes front and back windows for pressure measurements and feedthrough hex wrenches for adjusting the clamping pressure while at high temperature.

The DAC was loaded and lightly clamped for a pressure of 10–15 kbar. The cell was then placed in the vacuum oven and the temperature raised to 400 °C. The cell clamp bolts were tightened as needed to counter pressure losses due to thermal expansions of the cell components. The sample was annealed for 1 h at high temperature to ensure that an altered equilibrium was established. The cell was then clamped to above 30 kbar, and cooled to room temperature. The DAC assembly was transferred to the refrigerator cold finger and cooled to 170 K. At this temperature the pressurizing bolts were loosened and the refrigerator vacuum shroud put in place, so the sample could continue cooling to 12 K. The pentane was lost in this procedure.

A XeCl excimer laser-pumped dye laser was used for fluorescence excitation. The dye laser had a typical line width of 0.15 Å , and pulse energies were reduced to 10 μJ with neutral density filters. Because of the long (22.5 ms) lifetime of the *O* site, a low repetition rate of 13 Hz was used. The beam was focused to about 150-μm width at the sample.

Fluorescence collection is restricted by the DAC geometry, and was done at 0° with respect to the incident beam. After filtering to remove laser scatter the fluorescence could either be focused onto a photomultiplier for broadband detection, or directed into a 1-m monochromator. Because of the small sample size, it was important to collect a wide angle of fluorescent light, and to minimize focusing aberrations. A compound lens with an effective numerical aperture of $f/1.7$ was used to produce a clear magnified image. A gated integrator with a preamplifier was used to process the signal, and the spectra were monitored and recorded by computer.

Excitation spectra with broadband detection were used to measure the intensities of the *A* and *O* sites. For the clusters and minor sites the monochromator was used at several spectral windows chosen for optimizing the specific sites. The *A* site appears in the excitation scans for all of the spectral windows because of its high concentration and broad phonon sidebands, and was an intensity reference for the other major and minor sites. Intensity ratios from the sample's spectra were compared to ratios from an untreated reference crystal. After measuring all of the sites, a strip heater on the refrigerator was used to heat the sample to a set temperature, where it was annealed for a 30-min interval. The sample was then cooled, and spectra were taken. The annealing proce-

dure repeated at increasing 5° temperature steps.

Several problems were encountered with taking spectra of the samples while they were inside the DAC, including damage to the diamonds. For pulse energies greater than 50 μJ with focused spot sizes smaller than 50 μm, laser damage marks and small chips appeared on the diamond culet face. This power level should have been safe for diamond, so the cause was more likely absorption by traces of gasket metal on the diamond faces or by substances left from the evaporation of the pressurizing fluid. This problem limited the focused laser power that could be used for sample excitation.

The reproducibility of the relative spectral line intensities was poor when the samples were inside the DAC. Etalon effects, or other problems related to the high refractive index of diamond, were probable causes of these inconsistencies, but there was no clear pattern. We also found that the relative peak intensities for large reference crystals varied with the thickness and thermal history of the crystal. These problems were addressed by transferring the pressure treated chip, while cold, out of the DAC and into a custom sample holder. The holder has several cavities, so a small reference chip could also be included, and the reference chip would experience the same annealing conditions as the sample.

Variations in the dye laser set a limit on the accuracy of the experiment. It was found that changes in the spatial heterogeneity of the laser beam could be minimized by frosting the entrance window of the sample holder. Using peak areas and averaging multiple scans, the standard error for the A/O site intensity ratio was typically 3% for DAC measurement and 1.5% using the sample holder with a frosted window. Ratios for the minor sites had standard errors from 4% to 10% depending on their concentration.

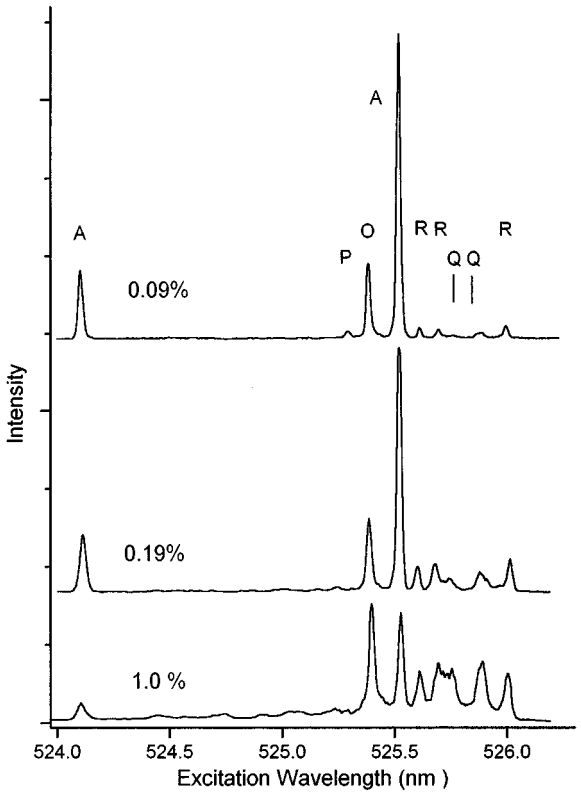

FIG. 1. Comparison of $^7F_0 \rightarrow {}^5D_1$ absorption spectra for samples of CaF_2:Eu with different dopant concentrations. All crystals were quenched from above 800 °C. The main defect sites are indicated.

RESULTS

Part I

An excitation scan for the 0.09% crystal, monitoring all fluorescence, is shown at the top of Fig. 1. The peaks for A, O, P, and R sites are labeled, as are the positions for the very weak Q site peaks. An example of a site selective fluorescence scan is shown on the left in Fig. 2. If the dye laser is positioned on any of the R site excitation peaks, this same fluorescence spectrum is observed. Similarly, if the monochromator is positioned on one of the R site fluorescence lines, a site selective excitation scan will show only the three R peaks in Fig. 1, and not the A, O, P and Q peaks.

Figure 3 (top) shows an enlarged view of the high end of the excitation scan. In addition to the main peaks, there are numerous small overlapping features located in the region between the second and third R peaks, as well as near both sides of the O peak. Fluorescence scans were recorded as the dye laser was stepped across these regions, to separate and correlate the features. Several minor sites were identified.

The fluorescence scan shown on the right in Fig. 2 was recorded with the dye laser at 525.32 nm, which is just below the excitation line for the O site. Four new sites, labeled $O1-O4$, were observed in this region, two of which are visible in the figure. These sites show two or three fluorescence lines lying close to, but split about the O site fluorescence line. In the excitation scans the sites also showed this type of close-splitting pattern. We suggest that these centers correspond to single europium ions, like the O site, except that they are perturbed, and the $O1$ site the least perturbed. At least two additional sites were observed at lower wavelengths, near the P site line. While this is in the spectral region where the other single sites are found, the nature of these sites is not known. An examination of the spectral region around the main A peak did not reveal similar line groups.

The spectral region between the R peaks is more complex. Spectra monitoring transitions to both the $^5D_1$ and $^7F_1$ manifolds have numerous overlapping lines. In the $^7F_0 \rightarrow {}^5D_1$ excitation scan four sites (labeled $M1-M4$) were clearly distinguished, and a fifth broader feature (labeled $M5$) was less clearly distinguished. In the fluorescence scans many of the lines could not be assigned with certainty to a specific site. Better instrumental resolution would allow further identification of sites, but this approach was not necessary for the experiments. We associate the sites in this region with europium clusters, based on the line positions, spectral splitting and fluorescent lifetimes. In crystals quenched from high temperature, clusters larger than dimers should be rare, which is consistent with the small amount of Q site seen in the spectra. Thus these clusters are probably perturbed-R sites or dimers having a different lattice configuration than the R site.

One additional significant site was observed which does not fit into these two categories. The site labeled N has excitation lines in both the ''single'' and ''cluster'' regions of the scan. Its $^5D_1$ fluorescence lifetime is more consistent

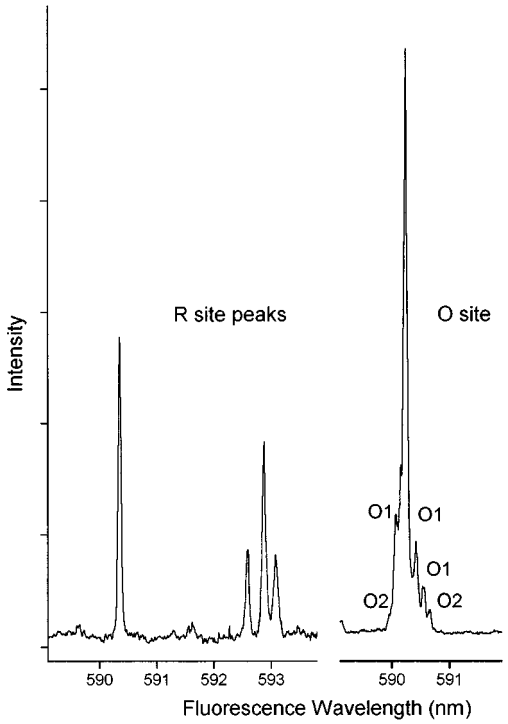

FIG. 2. Site-selective fluorescence spectra of various sites. Excitation was at 525.62 nm for the scan on the left, and at 525.30 nm for the scan on the right.

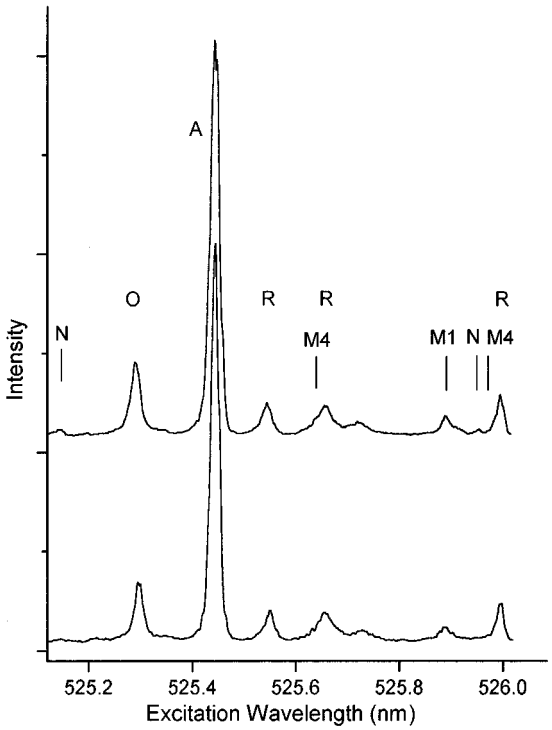

FIG. 3. Comparison of spectra from 0.19% CaF_2:Eu crystals before (top scan) and after high-pressure treatment. The main sites, and the affected minor sites, are indicated.

TABLE I. Wavelengths of spectral lines for defect sites in $CaF_2:Eu^{3+}$.

Site	Excitation $^7F_0 \rightarrow {}^5D_1$	Fluorescence $^5D_0 \rightarrow {}^7F_1$
O	525.34±0.01 nm	590.28±0.01 nm
A	524.15 525.51	588.93
R	525.62 525.71	590.37 592.51
	526.06	592.78 592.99
Q	525.51 525.78 525.91	590.53 591.76 593.47
N	525.15±0.01 nm	588.72±0.02 nm
	525.98	592.95 593.33
*M*1	525.82 525.93	591.55 593.30
*M*2	525.74 525.86	588.75 591.24
	525.96	591.57 593.43
*M*3	525.87	591.26 591.56
	525.92	591.95 593.02
*M*4	525.68	591.20 591.35
	526.02	591.88 593.80
*M*5	525.76	591.40 591.62 593.38

with a single ion site. At 12 K, lifetimes for the *O* and *A* sites are 3.5 and 3.6 ms.[9] Energy exchange processes in clusters cause shorter lifetimes, 25 and 15 μs, for the *R* and *Q* sites. For the minor clusters we found lifetimes in the hundreds of microseconds, but the *N* site was measured at 2.0±0.4 ms. One possibility is that the *N* site is a europium associated with an impurity. A summary of lines for the major and minor sites is given in Table I.

For the remainder of the experiments, four monochromator settings were chosen for measuring the relative site concentrations. The settings were chosen to contain fluorescent lines from more than one minor site, and to maximize spectral discrimination between selected sites. Figures 4 and 5 show scans using two of the settings. Except for the *M*1 site, there are measurable peaks with little or no overlap of other sites. For both *M*1 peaks it was necessary to estimate and subtract the contributions from smaller interfering peaks.

Crystals covering a range of dopant concentrations were available for the experiments. The spectrum of the 0.09-mole % Eu^{3+} crystal has been presented in Fig. 1. The spectra for crystals with 0.19% and 1.0% concentrations quenched from 890 °C are also given in the figure. A comparison of the spectra clearly shows the anomalous relation between the *A* and *O* sites, where the ratio of *A*/*O* decreases with increasing concentration. The intensity of cluster peaks is observed to be high in the 1.0% sample, despite the high quenching temperature. Also noticeable is an increase in numerous uncharacterized peaks between the first *A* peak and the *O* peak. These peaks presumably arise from perturbed single ion sites.

Part II

The 0.19% Eu crystal was chosen for the detailed annealing experiments. The spectra presented here are for a chip which was treated in the DAC at 420 °C and 11±3 kbar of pressure. The sample was transferred to a cavity on the sample holder, while two untreated crystals were placed in other cavities on the holder. No significant differences between the two reference crystals were observed.

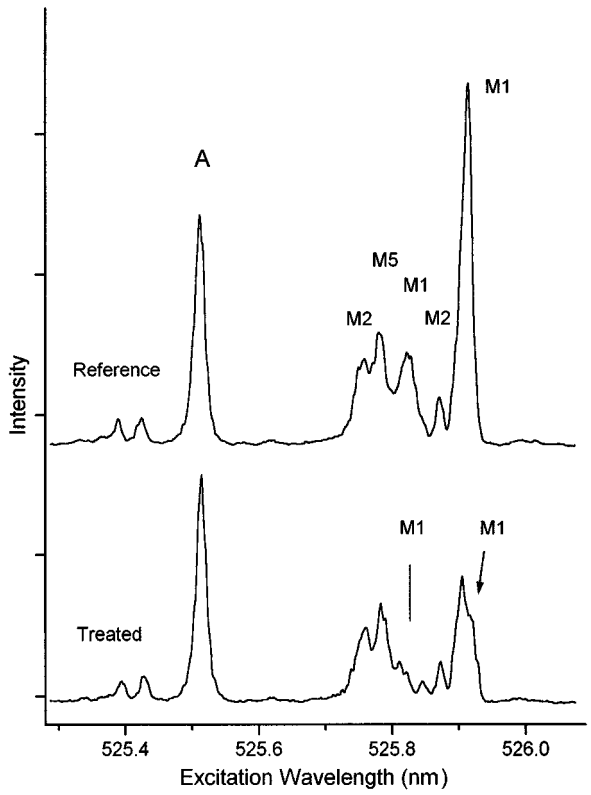

FIG. 4. Site-selective excitation spectra showing the pressure induced change in the $M1$ site. The A-site line was used for calculating the amount of change.

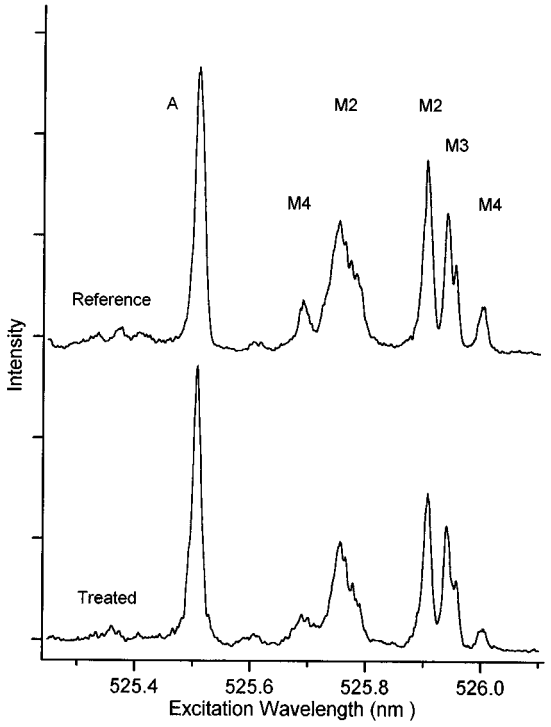

FIG. 5. Site-selective excitation spectra showing the pressure induced change in the $M4$ site.

Excitation spectra of the sample and reference are given in Fig. 3. The most noticeable difference after the pressure treatment is a decrease in the O peak. The A/O ratio for the sample is 24% greater than that of the reference. The A and the O sites are related by the gain or loss of a local interstitial fluoride, so that a decrease in the O site should be accompanied by an increase in the A site. Using the R peaks as constant features for comparison purposes (the R site appears to remain constant in all of our work) the A/O change can be broken down into a 19% decrease in the O peak and a 5% increase in the A peak. Taking into consideration the peak sizes and the instrumental response for the two sites, these changes represent comparable absolute amounts.

In the Fig. 3 spectra, some of the minor peaks have diminished in intensity, as marked on the figure. Site-selective spectra were used to quantify these changes. Spectra of the treated sample are presented in the lower portion of Figs. 4 and 5. Comparing these spectra to the reference spectra shows that the $M1$ site has experienced a 90% reduction, and the $M4$ site has decreased 45%. Sites $M2$, $M3$, and $M5$ have not changed. Other scans show that the N site experienced a 40% reduction.

The minor cluster sites should have conjugate sites which would increase as the clusters decrease; however, no such sites were observed. It is possible that the conjugate features for the minor clusters are spectrally indistinguishable from other sites in the crystal.

A number of preliminary experiments were done using the 0.09% Eu crystal. The treated samples consistently showed a 10–14 % increase in A/O ratio. Site-selective scans and a reequilibration anneal were done on one of the samples. The results were similar to those shown for the 0.19% Eu crystal, but there was also a reduction in the $M5$ site.

The preliminary sample treatments were tried with various combinations of DAC pressure and temperature. When the initial DAC annealing pressure was greater than 20 kbar at 400 °C, the experiments failed to produce any changes in the sample, indicating that the fluorides were not mobile. Studies on the relaxation of bound defects show that the increase in the diffusional activation energy at these pressures is modest,[16] so an increase in the association energy of the sites is probably the main reason for this lack of mobility.

Part III

Reequilibration of the pressure-treated sample was performed by a series of 30-min anneals at increasing temperatures. The recovery of the sample A/O ratio, compared to the reference, is plotted against annealing temperature in Fig. 6. The improvement in the experimental precision at 300 K corresponds to the insertion of the frosted window on the sample holder. The plot shows recovery beginning around 290 K, with equilibrium fully reestablished at 355 K.

The site-selective spectra showed the recovery of the minor sites begins around 270 K. The results for the $M1$, $M4$, and N sites are shown in Fig. 7. Each minor site is different in its annealing behavior. Their recovery rates, at any given temperature, do not seem correlated.

The reference crystal also showed changes in its site concentrations above 300 K. The temperature record for the val-

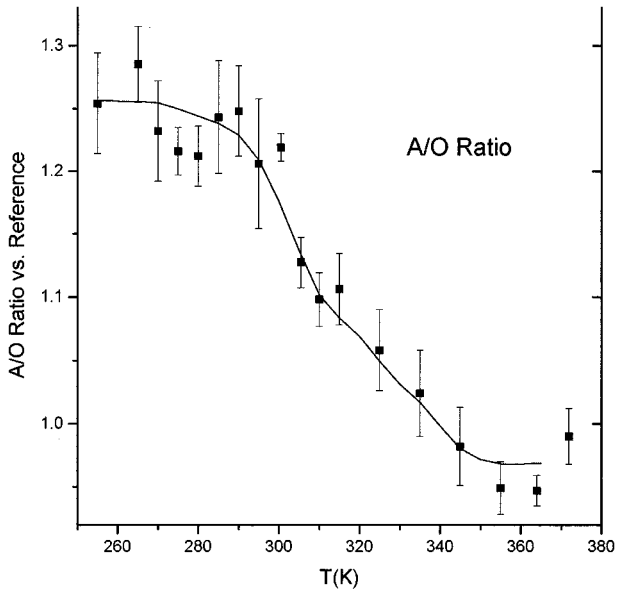

FIG. 6. Annealing history of the A/O ratio for the reequilibration of the pressure-treated crystal at 1-atm pressure relative to a reference crystal that was not exposed to high pressure but was annealed under identical conditions. Each point represents a 30-min anneal. The line shows the result of the computer simulation.

ues of the A/O ratio and the $M1/A$ ratio are shown in Fig. 8. The growth of the $M1$ feature and decline in the A site above 320 K suggests that there are substantial differences in the entropy of association for the sites. Since the reference chip was annealed alongside the sample, these variations are not a problem for this experiment.

DISCUSSION

For CaF_2 doped with trivalent rare earths, and free of other contamination, the excess cation charge is compensated for by interstitial fluoride ions. For low dopant concentrations the defect chemistry has traditionally been interpreted in terms of the dissociation of rare-earth–interstitial-fluoride pairs. For europium the relations are

$$\mathrm{Eu}\cdot\mathrm{F}\leftrightarrow\mathrm{Eu}^{\cdot}+\mathrm{F}_i', \tag{1}$$

$$\frac{C_O C_{\mathrm{F}}}{C_A}=\exp(-g_a/k_BT), \tag{2}$$

where k_B is Boltzman's constant, C_A and C_O are the concentrations of the A and O sites in mole fraction, and C_{F} is the concentration of free interstitial fluorides. At room temperature g_a is around 0.6 eV,[2,3] so the amount of dissociation is small, and the concentration of C_A is comparable to the total dopant concentration C_{Eu}. Solving Eq. (2) gives,

$$C_O=C_{\mathrm{F}}=(C_{\mathrm{Eu}})^{1/2}\exp(-g_a/2k_BT). \tag{3}$$

This model for the defect chemistry has serious limitations. For dopant concentrations above 0.01 mole % it does not address defect clustering or other factors contributing to the anomalous O site concentration dependence. For concentrations below 0.01%, impurities and intrinsic defects become important. Equation (3) predicts lower C_O values than are actually observed (5).

The doping process introduces matching amounts of rare-earth ions and F_i' ions. Each europium atom can trap an interstitial fluoride. Interstitials can also be trapped by europium clusters, impurities, and intrinsic defects. Due to these additional traps, the number of potential trap sites is always larger than the number of interstitial fluorides in the doped crystals. This leads to a competition between sites for the interstitial fluorides.

We propose a model for the distribution of interstitial fluorides which includes the effects of competing equilibria. While the majority of interstitial fluorides will still be trapped by europium defects to form A sites, other traps with higher association energies will bind preferentially. As a result, many of the europium defects will not be locally compensated. The crystal will have a significant concentration of an O site, even though C_F remains small. Solving Eq. (2) in this case gives

$$C_F=\frac{C_A}{C_O}\exp(-g_a/k_BT). \tag{4}$$

Measurable amounts of both the A and O sites are found in all moderately doped samples. The concentration of free fluorides is therefore well regulated by Eq. (4), and is effectively determined by the A site association energy g_a. For an association energy of 0.6 eV, and C_A equal to C_O, Eq. (2) predicts C_F will be $\sim 4\times 10^{-11}$ at room temperature.

The ability of other trap sites to retain interstitial fluorides will be determined by how their association energy compares to g_a. A trap site T with an association energy significantly greater the A site will be found in the associated form, $T\cdot\mathrm{F}'$. An example of this stability is the R site $(2\mathrm{Eu}\cdot 3\mathrm{F})'$, which was not affected by the pressure and heat treatments in this experiment. The unassociated form, $(2\mathrm{Eu}\cdot 2\mathrm{F})^x$, is not known to occur. Conversely, sites with an association energy significantly lower than g_a, such as the postulated $(\mathrm{Eu}\cdot 2\mathrm{F})'$ site in CaF_2, should not be expected to form.[7,17] Another example of a site which would not retain fluorides is a rare-earth–interstitial dipole strained by another nearby defect, for which computer modeling predicts a considerably lowered fluoride association energy.[18] The set of minor sites located around the O site in the spectra may correspond to these perturbed sites.

Traps with free energies of association similar to that of the A site will effectively compete with it for interstitial fluorides, and will be partially found in the associated form. Partially associated sites must have association energies within $\sim 2k_BT$ of the A site; at room temperature this energy difference is 0.05 eV. An example is the $M1$ site, the concentration of which is affected by changes in both temperature and pressure. The $M4$ and N sites must also have association energies comparable to the A site.

Because the association energy for the various sites will have different contributions from entropy, strain, and Coulombic forces, the high pressure and temperature treatment shifts the stability of sites relative to that of the A site. This leads to the altered high-pressure distribution of the fluo-

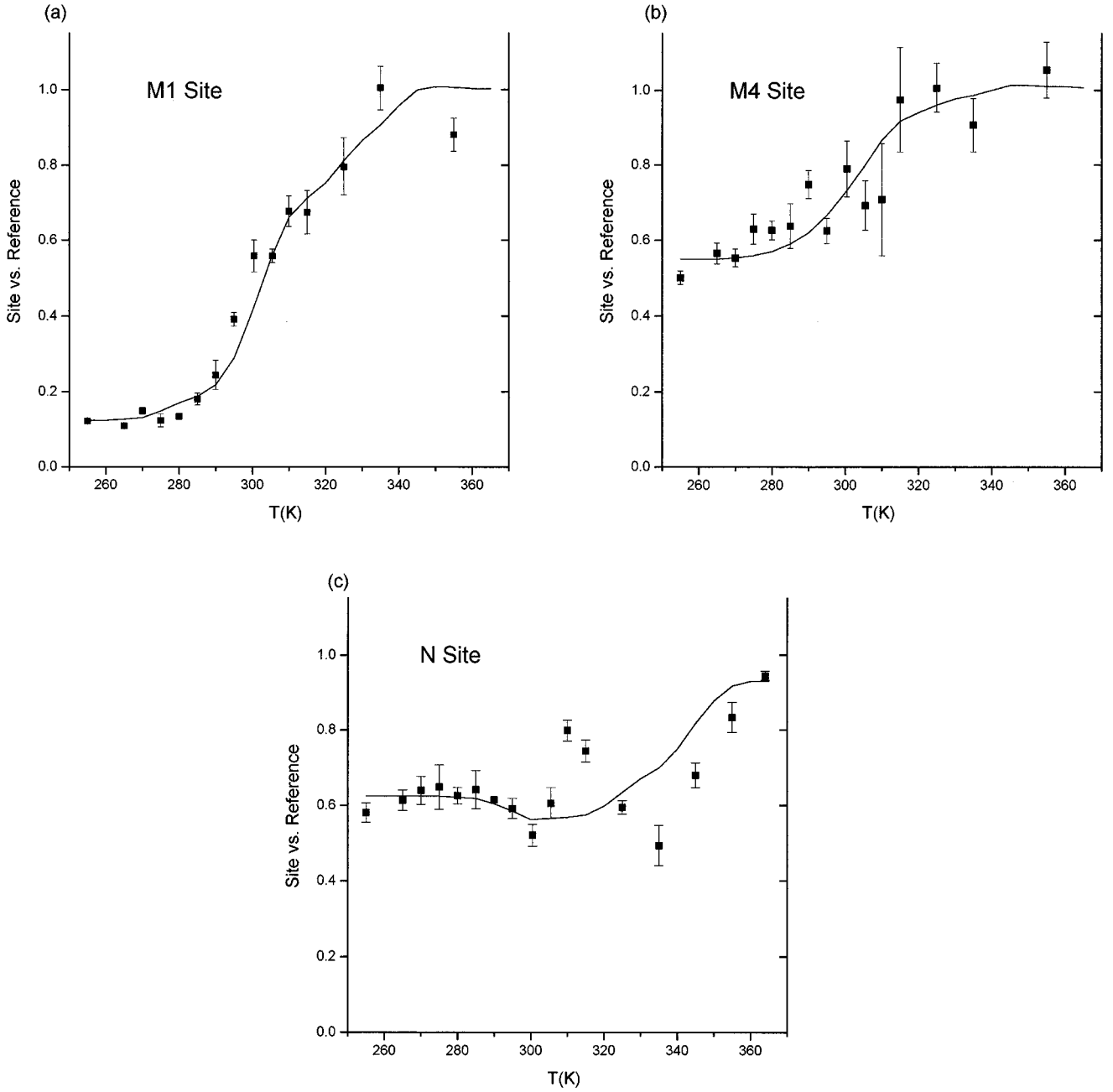

FIG. 7. Annealing history of (a) the $M1$ site, (b) the $M4$ site, and (c) the N site measured relative to an identical reference crystal that was not exposed to high pressure but was annealed under identical conditions. The lines show the result of the computer simulation.

rides. The reduced mobility of the fluorides at high pressure suggests that the association energy of the sites generally increases with pressure.

A computer simulation of the low pressure reequilibration was used to obtain kinetic information from the data. To model the multiple competing equilibria, the simulation allowed several different trap sites to interact. For any trap site, an equilibrium can be written

$$T_n\cdot\mathrm{F}\leftrightarrow T_n^{\cdot}+\mathrm{F}_i', \tag{5}$$

where $T_n\cdot\mathrm{F}$ represents any site with a labile fluoride. For the simulation, the A site and the minor sites $M1$, $M4$, and N were included. T_n represents the O site and the conjugate forms of the minor sites. The forward reactions produce a flux of interstitial fluorides, $J_f(n)$, leaving the traps and entering the free lattice. Similarly, the reverse reactions produce a flux of fluorides leaving the free lattice, $J_r(n)$. The fluxes are determined by the rate equations for the forward and reverse reactions,

$$J_f(n)=C_{T\cdot\mathrm{F}(n)}k_f, \tag{6a}$$

$$J_r(n)=C_{T(n)}C_{\mathrm{F}}k_r. \tag{6b}$$

The reverse reaction is a diffusion-controlled process, with the traps acting as sinks for interstitial fluorides. The Smoluchowski model can be used to obtain values for the rate[19]

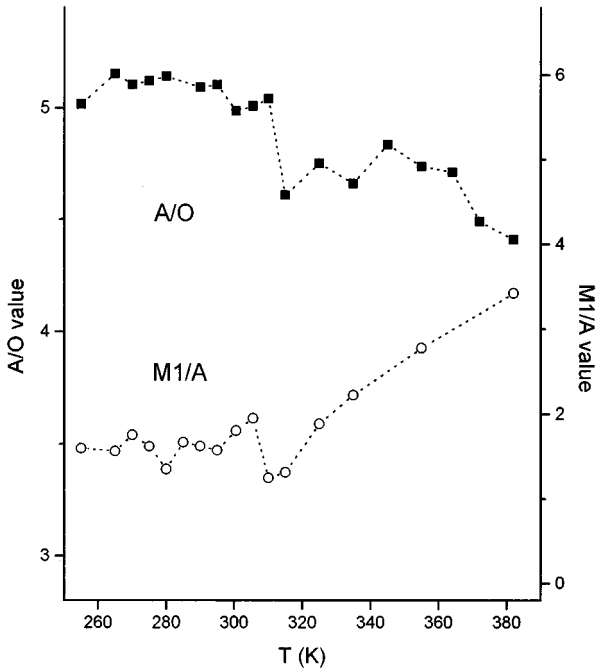

FIG. 8. Changes in the A/O and $M1/A$ ratio values of the reference crystal after annealing.

$$k_r = 4\pi(D_T + D_F)(R_T + R_F), \tag{7}$$

where D_T and D_F are the diffusion constants for the traps and the interstitial fluorides. For temperatures below 530 °C cations are not mobile, so D_T is zero. $R_T + R_F$ is the effective reaction radius between traps and fluorides. Coulombic and strain forces extend a considerable distance from a defect site, but the forces fall off rapidly with distance. For the simulation, the reaction radius was set at one lattice spacing. This choice is consistent with using only nearest-neighbor positions for determining the spatial degeneracy of a defect site.[3]

For diffusion in a cubic lattice,

$$D_F = \frac{d^2}{2}\nu_0 \exp(g^*/k_B T), \tag{8}$$

where g^* is the activation energy for diffusion of the interstitial fluorides. For the attempt frequency ν_0, the frequency of an optical phonon mode is used.[3] d is the length for a diffusive jump in the (110) lattice direction. When using mole fraction as the concentration unit, the simple unit cell is assigned a volume of one unit, which gives a value for d of 1.12 units of length. Combining Eqs. (6b), (7), and (8) gives

$$J_r(n) = C_{T(n)} C_F 4\pi \frac{d^2}{2}\nu_0 \exp(-g^*/k_B T). \tag{9}$$

The forward reaction is a diffusion controlled dissociation process. The rate equation governing this process can be derived from the relationship between the rate constants and the equilibrium expression for the dissociation of site n:

$$K_{eq} = \frac{k_f}{k_r} = \exp[-g_a(n)/k_B T]. \tag{10}$$

An expression for k_f can be obtained, and substituted into Eq. (6a) to obtain an equation for the forward reaction rate. Separating the free-energy terms into enthalpy, vibrational entropy, and the spatial degeneracy z, the equations for the forward and reverse fluxes are

$$J_f(n) = C_{T\cdot F(n)} 4\pi \frac{d^2}{2}\nu_0 \frac{z_i}{z_T} \exp\{(s^* + s_a)/k_B - [h^* + h_a(n)]/k_B T\}, \tag{11a}$$

$$J_r(n) = C_{T(n)} C_F 4\pi \frac{d^2}{2}\nu_0 \exp(s^*/k_B - h^*/k_B T). \tag{11b}$$

For an interstitial site, z_i is one, and for the A site, z_T is 6. This z_T value was also used for the minor sites. For s^*, s_a, and ν_0, Bollmann's values of $5.57k_B$, $4.42k_B$, and 7.4×10^{12} s^{-1}, respectively, were used.[3] The concentration of each of the four sites, along with the fraction of each site starting in the associated form, were fitting parameters for the simulation. These parameters determine the starting values for $C_{T\cdot F(n)}$ and $C_{T(n)}$ in the simulation.

These experiments cannot separate the contributions of h_a and h^* to the total Arrhenius energy E. Since each site will vary slightly in its value for h_a, the sites will have different values for the Arrhenius energy. For fitting parameters, a value of E representing the A site was used, along with $\Delta E(n)$ values for each of the minor sites:

$$E(n) = E + \Delta E(n) = h^* + h_a(n). \tag{12a}$$

For the simulation there are advantages in treating h_a, the association enthalpy for the A site, as a constant, rather than fixing the value of h^*. The value for h^* is then expressed as

$$h^* = E - h_a. \tag{12b}$$

In addition to the specified values and the fitting parameters, the equations contain two unknown values h_a and C_F. These unknown terms can be eliminated by using the relationship between the forward and reverse fluxes. The concentration of free interstitial fluorides is always small, so the steady-state approximation applies to C_F. The sum of the rates for all of the forward reactions must equal the sum of the reverse rates. The summation for the forward reactions can be explicitly done. For the reverse reactions, h_a is constant, and it can be moved outside of the summation. During the reequilibration, C_F may vary from its equilibration value, but it will be the same for all sites and can also be factored out of the summation. The equations for the simulation become

$$\Sigma J_f(n) = \Sigma J_r(n), \tag{13a}$$

$$\Sigma J_f(n) = \Sigma C_{T\cdot F(n)} 4\pi \frac{d^2}{2}\nu_0 \frac{z_i}{z_T} \times \exp[(s^* + s_a)/k_B - (E(n))/k_B T], \tag{13b}$$

$$\Sigma J_r(n) = [C_F \exp(h_a/k_B T)]\Sigma C_{T(n)} 4\pi \frac{d^2}{2}\nu_0 \times \exp[s^*/k_B - E/k_B T]. \tag{13c}$$

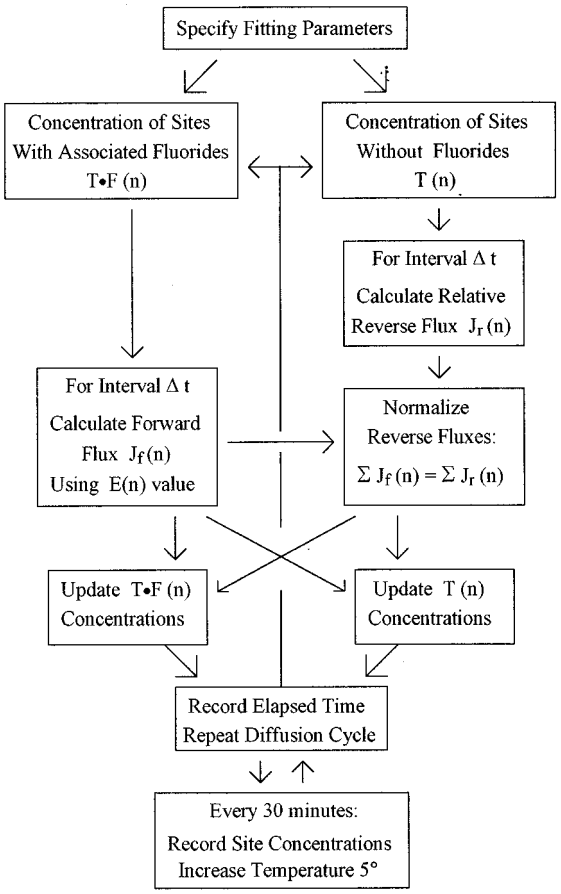

FIG. 9. Block diagram of the computer program used to simulate the reequilibration anneal.

The value of $[C_F \exp(h_a/k_B T)]$ can be found by equating Eqs. (13b) and (13c). With this information, individual values for the reverse rates can be found for each site.

Using the explicitly calculated forward rates, and the derived reverse rates, the simulation calculates the changes in each site for small time intervals:

$$C_{T\cdot F(n)}(t+\Delta t) = C_{T\cdot F(n)}(t) + (\Delta t)[J_r(n) - J_f(n)],$$
$$C_{T(n)}(t+\Delta t) = C_{T(n)}(t) - (\Delta t)[J_r(n) - J_f(n)]. \quad (14)$$

A block diagram of the simulation program is given in Fig. 9. The input parameters are the concentration of each type of site, $C(n)$, the initial fraction of each site found in the associated form, the Arrhenius energy for diffusion by the A site, E, and the variation of diffusion energy for each of the other sites, $\Delta E(n)$. The calculation of the relative reverse reaction fluoride fluxes uses arbitrary values for h_a and C_F. The comparison to the explicitly calculated forward fluxes in the following step is used to obtain correct reverse values. The size of the time interval, Δt, was adjusted as needed during the simulation so that the diffusion from or into a site never exceeded 5% of the site's concentration.

It was found that the experimental reequilibration curves could not be reproduced using a single enthalpy value $E(n)$ for each other europium sites; using single values gave recovery of the site ratios over approximately a 30° temperature range. To give the 80° range observed in the experiment, it was necessary to partition each of the europium sites into several regions with different diffusional enthalpies.

TABLE II. Parameters for diffusional enthalpies and defect distributions used in the reequilibration simulation.

Diffusion enthalpy for A/O sites (ev) Lattice region/Defect populations			
1	2	3	4
1.18	1.31	1.41	1.52

Comparison of Simulation Features

Site	Relative amount	Energy vs main feature	Initial gettered fraction	Fraction in lattice region: 1	2	3	4
A/O	22.0	0.0 eV	0.70	0.003	0.070	0.080	0.847
$M1$	1.0	+0.01	0.10	0.40	0.60	0	0
$M4$	0.3	+0.05	0.45	0.40	0.60	0	0
N	0.5	−0.01	0.40	0	0.50	0	0.50

Equations (12) and (13) can be modified to include different diffusion regions. Instead of one value for E, values must be specified for each of the regions. Additional fitting parameters are needed to specify the fraction of each site placed in each of the regions. The value of h_a remains constant, and it can still be factored out of the summation. Since the spectra cannot distinguish between regions, the total amount for each site is used to compare the simulation to the experimental data.

To model the reequilibration data, a range of activation energies spanning 0.34 eV was needed. The simulation plots shown in Figs. 6 and 7 were produced using activation energies (for the main site) of 1.18, 1.31, 1.41, and 1.52 eV. The best fit to the data was obtained by concentrating most of the minor site populations in the lower activation energy regions, and most of the A and O sites in the higher activation energy regions. This result is consistent with the idea that clustered portions of the lattice would also be regions of higher lattice strain and increased mobility.[20] The parameters used in the simulation are listed in Table II.

The lowest activation energy region was required to simulate the recovery of the minor sites. The minor sites show recovery beginning at approximately 270 K, appreciably lower than the temperature observed for the A/O ratio. A small fraction of the A-O site was needed in the lowest energy region to model the minor site recovery, but the amount was below the accuracy limits for the A-O data, so the A/O ratio does not significantly reflect this energy region. For the N site, the best match was obtained when the europium site was distributed in both high and low enthalpy domains, but the N-site data could still not be accurately fit using this simulation.

The existence of regions with differing diffusion energies helps explain discrepancies in the existing literature on fluoride mobilities. Bulk measurements will be influenced by both slow and fast processes in a sample, but should generally reflect the higher-energy barriers to diffusion. Bollmann's results for conductivity in the low-temperature asso-

ciation region had an Arrhenius energy of 1.27 eV in CaF_2:Y.[3] Using calculated association energy values for yttrium and europium to compare the two systems,[7] this is equivalent to 1.39 eV in CaF_2:Eu. This value is consistent with the higher-energy regions in our experiments. In a photobleaching experiment, Twidell proposed that free interstitial fluorides were returning to trap sites.[21] He obtained a value for h^* of 1.0 eV. Adding an association enthalpy term h_a of approximately 0.6 eV to this, as in Eq. (7), also places this result at the high end of our energy range. Conductivity and self-diffusion experiments at high temperature, where the F_i' are dissociated, gave similar results.[3,22]

Experiments measuring local mobility, however, should reflect the lower-energy pathways. In a fluorine NMR experiment, Wei and Ailion found an Arrhenius energy of 1.04 eV.[4] Assuming this value measured the combined diffusional and association energies, it is in good agreement with what we found for strained lattice regions.

CONCLUSION

The results of this experiment show a defect chemistry which is much richer and more complex than has previously been assumed in interpreting experimental results. A model for defect distribution and fluoride diffusion has been proposed which is consistent with the main experimental results. The concepts of strained lattice regions, and competing equilibria between sites for the interstitial fluorides are essential for explaining our observations.

Within a single sample, the fluoride interstitial mobility had activation energies covering a 0.34-eV range. This range helps explain why previous experiments have given different results for fluoride mobility. Experiments measuring bulk properties will give higher values than experiments probing local effects, since the more restricted diffusional jumps must be included in the overall process. The observed relationship of the cluster sites to the strained regions in the crystal suggests that samples with different preparation histories may also give different experimental results.

The model presented here involves an interesting approach to the equilibrium between the rare-earth sites and the interstitial fluorides. Previously, a simple mass action relationship between defects and interstitial fluorides has been used to interpret results, and the competing equilibria from other sites have not been included in the calculations. The results of this experiment suggest that the competing equilibria are a dominant factor, and that the concentration of free interstitial fluorides is determined by the concentration of clusters and other fluoride traps in the sample.

The high-pressure techniques and site-selective spectroscopy presented here have shown an ability to extract information about local structure and dynamics not possible with other methods used for studying these systems. Future experiments should examine how differences in the observed properties of samples correlate with local defect structures. An understanding of these relationships should enable better control and optimization of the defect chemistry and ion conductivity in crystals.

ACKNOWLEDGMENTS

Acknowledgment is made to the Donors of The Petroleum Research Fund, administered by the American Chemical Society, for the support of this research. Support was also provided by the National Science Foundation under Grant No. DMR-9305849.

*Present address: Asbury College, Wilmore, KY.
†Present address: China Lake Weapons Laboratory, China Lake, CA.
‡Author to whom correspondence should be addressed.

[1] C. G. Andeen, J. J. Fontanella, M. C. Wintersgill, P. J. Welcher, R. J. Kimble, Jr., and G. E. Matthews, J. Phys. C **14**, 3557 (1981).
[2] C. R. A. Catlow, A. V. Chadwick, and J. Corish, J. Solid State Chem. **48**, 65 (1983).
[3] W. Bollmann and R. Reimann, Phys. Status Solidi **16**, 187 (1973).
[4] S. H. N. Wei and D. C. Ailion, Phys. Rev. B **19**, 4470 (1978).
[5] P. P. Yaney, D. M. Schaeffer, and J. L. Wolf, Phys. Rev. B **11**, 2460 (1975).
[6] D. S. Moore and J. C. Wright, J. Chem. Phys. **74**, 1626 (1981).
[7] J. Corish, C. R. A. Catlow, P. W. M. Jacobs, and S. H. Ong, Phys. Rev. B **25**, 6425 (1982).
[8] K. M. Cirillo-Penn and J. C. Wright, Phys. Rev. B **41**, 10 799 (1990).
[9] R. J. Hamers, J. R. Wietfeldt, and J. C. Wright, J. Chem. Phys. **77**, 683 (1982).
[10] C. W. Rector, B. C. Pandey, and H. M. Moos, J. Chem. Phys. **45**, 171 (1966).
[11] W. Gettman and O. Gries, J. Solid State Chem. **26**, 255 (1978).
[12] F. J. Gustafson and J. C. Wright, J. Anal. Chem. **51**, 1762 (1979).
[13] Diacell Products, Leicaster, England.
[14] A. S. Zinn, D. Schiferl, and M. F. Nicol, J. Chem. Phys. **87**, 1267 (1987).
[15] G. J. Piermarini, S. Block, and J. D. Barnett, J. Appl. Phys. **44**, 5377 (1973).
[16] M. C. Wintersgill, J. J. Fontanella, J. Welcher, A. V. Chadwick, and C. G. Andeen, Solid State Ionics **5**, 585 (1981).
[17] J. H. Crawford, Jr. and G. E. Matthews, Jr., Semiconduct. Insulators **2**, 213 (1977).
[18] D. G. Byrne, J. Corish, and D. A. MacDonaill, J. Chem. Soc. Faraday Trans. **86**, 1193 (1990).
[19] D. F. Calef and J. M. Deutsch, Ann. Rev. Phys. Chem. **34**, 493 (1983).
[20] H. W. den Hartog and J. Meuldijk, Phys. Rev. B **29**, 2210 (1984).
[21] J. W. Twidell, J. Phys. Chem. Solids **31**, 299 (1970).
[22] H. Matzke, J. Mater. Sci. **5**, 831 (1970).